VILNIUS TECH
Vilnius Gediminas Technical University

AVIATION
ISSN: 1648-7788 / eISSN: 1822-4180
2022 Volume 26 Issue 2: 96–103
https://doi.org/10.3846/aviation.2022.16886

LABYRINTH SEAL CFD CALCULATION AND TEMPERATURE MEASUREMENT INVESTIGATION

Michal ČÍŽEK [1*], Vojtěch KLÍR [2],
Pavel STEINBAUER [3], Tomáš VAMPOLA [1]

[1]*Center of Aviation and Space Research, Faculty of Mechanical Engineering, Czech Technical University in Prague, 16000 Prague, Czech Republic*
[2]*Vehicle Center of Sustainable Mobility, Faculty of Mechanical Engineering, Czech Technical University in Prague, 16000 Prague, Czech Republic*
[3]*Division of Mechanics and Mechatronics, Faculty of Mechanical Engineering, Czech Technical University in Prague, 16000 Prague, Czech Republic*

Received 7 December 2020; accepted 20 September 2021

Abstract. This article presents currently obtained results from CFD analysis of the labyrinth seals of an aircraft turbine engine. The process of describing a geometry, grid for numerical calculation and boundary conditions are described. Numerical simulations were performed for the assumed boundary conditions. The presented results show total temperature differences in labyrinth seals compared to published results. An experimental verification of the CFD analysis was also performed to clarify the numerical simulation results. It was based on the labyrinth seal measurement stand. The final part of this study is dedicated to the discussion and the following possible activities on this topic.

Keywords: aircraft turbine engine, labyrinth seal, simulation, measurement, total temperature, static pressure.

Introduction

Labyrinth seals are an essential part of the engine with a direct influence on the performance parameters. These parts operate under demanding conditions, mainly high temperatures and high-pressure ratios. This study describes the flow in the aircraft turbine engine labyrinth seal and the subsequent results obtained by computational fluid dynamics (CFD) calculation. Results were compared with outputs from the measurements from the dedicated test stand.

The labyrinth seal prevents a flow in secondary air system of aircraft turbine engine. But there is certain level of risk because of free cavity occurrence. This effect is generated between rotating and non-rotating parts, e.g., between the rotating shaft and shaft case (Sultanian, 2018). It can further result in low machine performance. There is a good reason for creating the most sophisticated design of labyrinth seals applicable to aircraft engines (Kurzke & Halliwell, 2018).

The labyrinth seal is contactless sealing. In general, contact sealing like piston rings or other rings (Romanik et al., 2019) are used. The disadvantage of contact seal is that it cannot be directly applied in turbomachinery because of high speeds and temperatures. In turbomachinery should be the blades, e.g., on top of the rotor, to prevent flow out of blades or in the rotating shaft where contactless sealing is necessary. The labyrinth seal hardware is often used and popular in engineering. The preliminary study was conducted with steam turbines (Fürst, 2016). Differences between steam turbines and aircraft turbine engines or gas turbines are in the magnitude of rotational speed. The rotational speed of the steam turbine is approx. 5000 rpm (Ščeglajev, 1983; Bloch & Singh, 2009). In the aircraft turbine engine is approx. 40000 rpm (Sultanian, 2018; Kurzke & Halliwell, 2018; Kerrebrock, 1992). This difference is used to assess the airflow in the labyrinth seal because the difference and quality of sealing has a thermodynamic performance parameters influence (Kurzke & Halliwell, 2018; Kmoch, 2002). It is also appropriate to explain how the seal works. The labyrinth seal consists of several cavities separated by teeth (Sultanian, 2018), where circumferential swirl loses kinetic energy (Čížek et al., 2020a). There are two approaches how to design the labyrinth seal for the aircraft engine. The first approach is

*Corresponding author. E-mail: *michal.cizek@fs.cvut.cz*

to design the labyrinth seal on the rotating part, e.g., on the shaft, and the second is to locate the seal on the non-rotating part.

Today, the airflow numerical simulations are frequently used. Firstly, the 1D algebraic methods were used to describe labyrinth seal behavior (Martin, 1908). The significant expansion of simulation technologies was based on the advancement of computers themselves. Currently, simulation can be performed in different physical depths based on available information and powerful computers. The CFD technology is a calculation method that works with Navier-Stokes equations (Ansys, 2016; Chorin, 1968). The previous study related to labyrinth seals was using steam turbine boundary conditions (Fürst, 2016). Another study where the labyrinth seal profile was analyzed is in Ilieva (2016).

Numerical investigation of the thermodynamic parameters with high rotating speeds were analyzed is in Jia et al. (2019). The preliminary study dealing with combinations of rotor teeth and high rotational speed is presented in Čížek and Pátek (2020). In this paper, the used calculation method is described. A study comparing rotor and stator teeth in higher rotational speed is stated in Čížek et al. (2020b). The influence of labyrinth seal teeth positions was also analyzed there. Results from both papers are that the total temperature increased, and the mass flow was eliminated through the labyrinth seal. It is the primary reason why the labyrinth seal is used in aircraft turbine engines and in all turbomachinery, e.g., gas turbines. However, the above result is from CFD analysis only and needs experimental validation. The labyrinth seal validation in a real aircraft engine was described in Čížek et al. (2020a). The particular measurement equipment was used in Tong and Kyu (2009). Another approach of labyrinth seal testing is in Campagnoli and Desando (2019), but the stepped non-rotating labyrinth seal was analyzed. The stepped labyrinth seal measurement capability was in Denecke et al. (2002).

The paper (Kerrebrock, 1992) describes the CFD study, where the boundary conditions correspond with aircraft turbine engine conditions. The motivation for this article was to verify the CFD calculation results with results from measurements. Previous research evaluated the calculated data by the real aircraft turbine measurement (Čížek et al., 2020a). Nevertheless, it is necessary to conduct an evaluation in a specific measurement device that fully corresponds with aircraft engine boundary conditions.

The article (Sultanian, 2018; Kurzke & Halliwel, 2018) states that the total temperature in the labyrinth seal is a constant value. This paper shows that the temperature in the labyrinth sealing is behaving quite differently, it increases.

The presented numerical results are validated by experiments on a test stand. Such as they are helpful for aircraft turbine design teams to consider material selection, stress, and fatigue properties properly.

1. Preliminary CFD study

The CFD calculation corresponds to the validation measurement. It follows from the result of (Čížek et al., 2020a) that the labyrinth seal's radial clearance (RC) is a dominant parameter. The RC is the area between the non-rotating wall and the tip of teeth. RC does significantly influence the good airflow sealing of labyrinth seal – the larger the RC, the larger the airflow and vice versa. When the RC is minimal, the air mass flow is minimal too. For a good comparison between CFD results and results from measurements, the proportional radial clearance (RCP) was defined by the following Equation (1):

$$RC_P = \frac{RC}{RC_{CH}}, \tag{1}$$

where RC_{CH} is the radial clearance in the flow channel (i.e. the area between rotating and non-rotating parts) without teeth.

2. Geometry description of CFD model

The geometry consists primary of 3 3D conical segments. The labyrinth seal volume (shown in Figure 1) is a non-rotating volume with a rotational wall (i.e., there are non-rotating teeth in the figure below) containing a constant number of teeth (i.e. #4 teeth in the Figure 1) and constant RC_P.

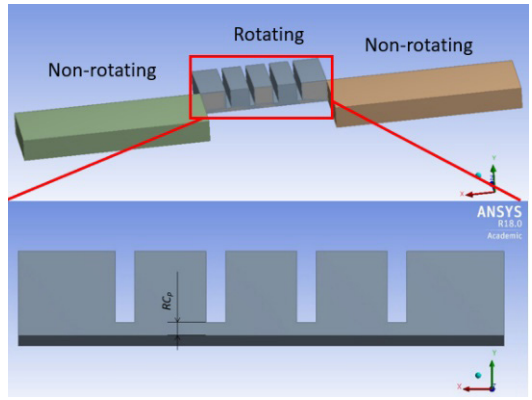

Figure 1. Geometry description

The inlet and outlet control volumes are defined in geometry for better stabilization of the airflow (the airflow direction is from left to right).

3. CFD calculation grid

The calculation grid is an important and necessary part that significantly influences calculation results. Before generating the grid, a quality analysis of 3 variants of mesh was created, which is in detail described in Čížek and Pátek (2020). Based on this result was created a special grid with 2.8 million cells and a Y+ value is 0.69. The hexahedral elements were used. Figure 2 shows a mesh of grid elements for the labyrinth seal domain. The influence

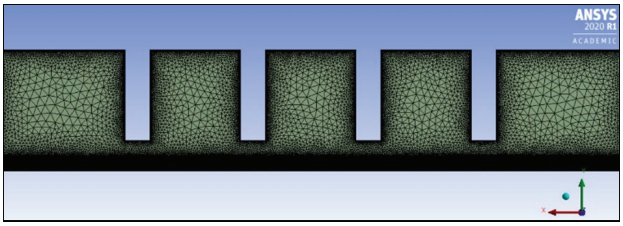

Figure 2. Grid elements used in calculation

function close to the wall describes airflow better, and the mapped grid methods were used. The commercial ANSYS Meshing software was used to define the grid. The Y+ value (ANSYS Help Viewer 18.0) and the number of cells and the fact that the grid inflation in all of the walls was used.

4. Boundary conditions

The computational model's boundary conditions setup fully correspond with the measurement device, i.e., non-rotating rectangle teeth and rotating smooth shaft (it is described in the next chapter). The CFD calculation was prepared in ANSYS CFX Pre software. The pressure of 0.25 MPa and temperature of 303 K were set up as inlet boundary conditions – see point 1 in Figure 3. The static pressure of 0.101325 MPa was set up as an outlet boundary condition (see point 2 in Figure 3). The periodic boundary conditions were set up on both sides of all rectangular domains – see in Figure 3. The shaft speed was defined as 35000 rpm. This speed corresponds with EASA type certificate of the turbo propeller engine – see (European Aviation Safety Agency, *Type Certificate Data Sheet,* 2014). The interface conditions were used between domains. The air ideal gas was set like a flow medium.

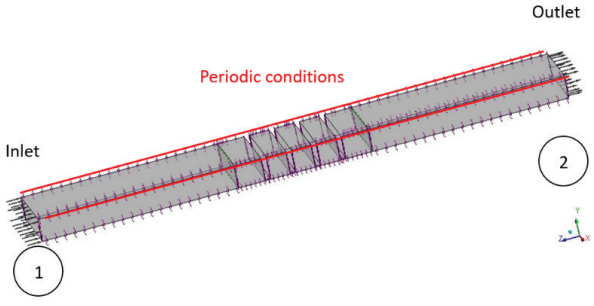

Figure 3. Boundary conditions

Based on the literature search (Čížek & Pátek, 2020), labyrinth seal calculation, Tong and Kyu (2009) – airflow calculation of labyrinth seal, Subramanian et al. (2015) – labyrinth seal airflow analysis, Selvaraji et al. (2007) – optimization of labyrinth seal, Stoff (1980) – numerical model and optical airflow measurement of labyrinth seal, Wu and Andrés (2018), labyrinth seal mass flow prediction (Ilieva & Pirovsky, 2019), the k-ε turbulent model in CFD calculation was selected. The variable timestep in ANSYS CFX Solver is listed in Table 1.

Table 1. Calculation timestep

Number of iterations	Timestep
1	1E-06
300	1E-05
500	1e-04

5. Calculation result

The calculation converged in 1000 iterations. The residual parameters (i.e., RMS P mass, RMS U-mom, RMS V-mom and RMS W-mom) were less than 1E-03. Before concluding, it is necessary first to define the evaluation parameters of the calculation. CFD calculation provides a lot of thermodynamic parameters. The calculation was made for two variants of radial clearance RC_P and 14 variants of rotating speed. A proper assessment of the aircraft turbine labyrinth seal is based on the static pressure (p_S) and total temperature (T_C) – Y-axis through the rotating speed (n) – X-axis. The calculated constant speed points from bottom to top indicate the number of teeth (i.e., in one constant speed row are four points because there are four teeth) in labyrinth seal.

As an example, velocity vectors with static pressure distributions are in Figure 4. The figure is from calculation where the rotating speed is n = 1000 rpm and RCp = 0.04. The figure shows, that the static pressure is decreasing, which means that the sealing through the labyrinth is working well. The velocity vectors show that the swirl is developed. This fact supports the previously stated.

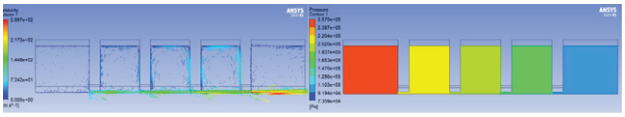

Figure 4. Velocity vectors and static pressure distribution

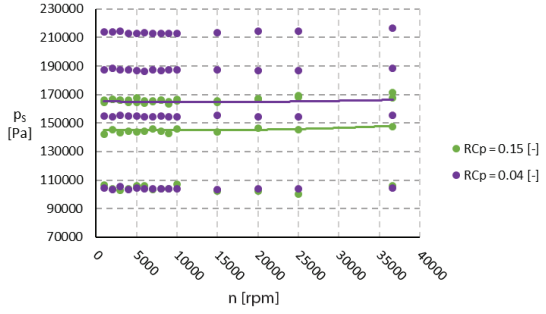

Figure 5. Static pressure trendlines

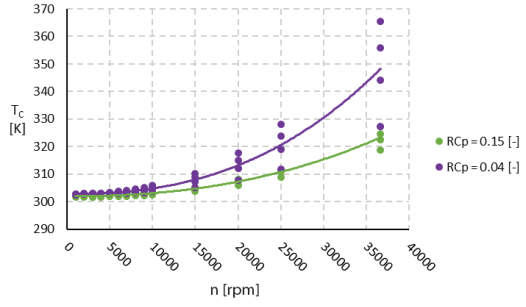

Figure 6. Total temperature trendlines

For further details, the static pressure difference Δp_S (based on Equation (2)) and total temperature difference ΔT_C (based on Equation (3)) were calculated.

$$\Delta p_S = p_{SL} - p_{SF}; \tag{2}$$

$$\Delta T_C = T_{CL} - T_{CF}, \tag{3}$$

where values with index L means the last teeth in the labyrinth seal and index F means the first teeth in the labyrinth seal.

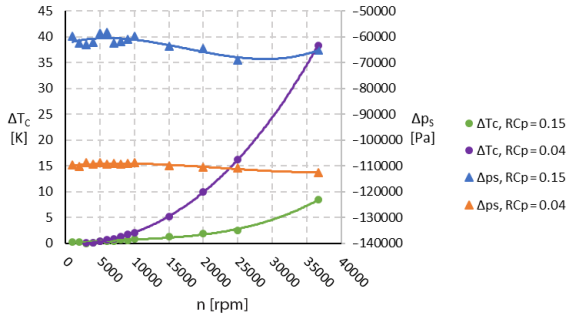

Figure 7. Static pressure and total temperature difference

In Figure 5 are shown static pressure trendlines through the labyrinth seal. In all of CFD result charts (from Figure 5 to Figure 7) are two trendlines – the first is for RCp = 0.04 and second for RCp = 0.15. As can be seen from the Figure 5, it is clear that the pressure degreasing with different rotating speeds is approximately constant. The main influence does have a radial clearance. In Figure 7 are shown the pressure differences (based on the Equation (2)). The difference values are negative because the static pressure in the first teeth is higher than in the last teeth.

In Figure 6 are total temperature trendlines through the labyrinth seal. From the trendlines, the total temperature increased with higher rotating speed and with smaller radial clearance. Figure 7 shows that with the highest rotating speed and the smallest radial clearance RC_P, the total temperature difference is 37 K and the static pressure difference is –110000 Pa. This finding contradicts the assumption in Sultanian (2018) and Kerrebrock (1992), especially that the total temperature is a constant value. It is a reason why evaluation measurement was prepared.

6. Labyrinth seal measurement

Because the CFD calculation results (absolute temperature difference) were novel and interesting for all engineering teams, it was necessary to obtain experimental data to confirm such statement. The experimental device was designed to test and measure the aerostatic bearings and the labyrinth seal by the CTU FME team from Department of Mechanics, Biomechanics and Mechatronics. This test stand was primarily designed for force measurements evaluated in the frequency domain. Therefore, it was necessary to upgrade the test device according to the planned activities.

6.1. Measurement device description

As mentioned in the previous chapter, the specialized test stand was used to physically model the behavior of the labyrinth seal under defined conditions. The fastening and setup system was adapted. Also, the testing device was instrumented according to requirements on acquired quantities for planned measurements. It mainly means to install temperature sensors on defined positions and to justify the mutual position of the stator and rotor.

The measurement device (Figure 8) consists of 3 parts:

1. The device case – It is a case in which is inserted the labyrinth seal body;
2. The labyrinth seal body – It is a body where are the non-rotating teeth;
3. The rotating shaft – It is a smooth shaft without teeth. The shaft is inserted into the labyrinth seal body and connected to the electrical motor via a clutch.

The measurement device is shown in Figure 8, where it should be visible the electrical motor (left side), the shaft with clutch (including the safety cover) and the device case (right side – red rectangle). The scheme of the device case (coarse hatching) is shown in Figure 9. The labyrinth seal body (fine hatching) was located on the stator of the testing device. The rotor was than designed like a smooth shaft (not in the picture). The pressurized air is distributed from the external compressor directly to the middle part

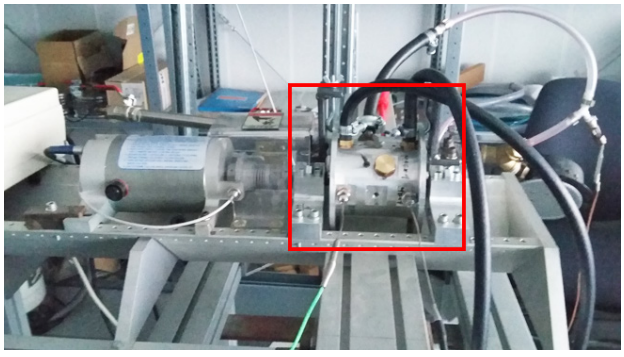

Figure 8. Measurement experimental device with red rectangle device case

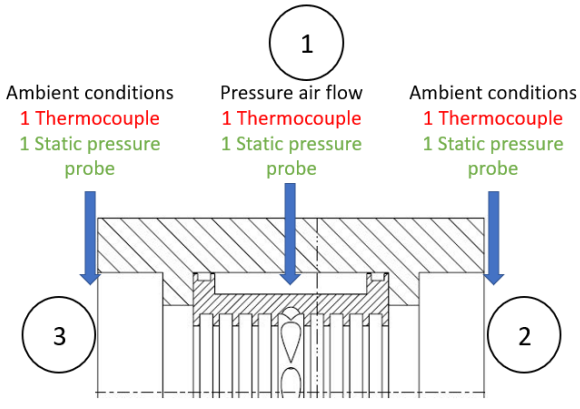

Figure 9. Measurement experimental device instrumentation scheme

of the labyrinth seal body. The flow passes to the teeth through the eight holes and is evenly distributed to both sides (left and right), expanding to the ambient environment. The total temperature and the static pressure were measured in the pressure inlet and on both sides (left and right positions).

The static pressure (p_{S1}) and inlet total temperature (T_{C1}) were measured in position 1. In points 2 and 3 the static pressures (p_{S2} and p_{S3}) and total temperatures (T_{C2} and T_{C3}) were measured. Ch-Ni Thermocouples type K with standard tolerance ±2.2 K (Childs, 2001) were used for temperature measurements. The static pressure tolerance was ±10 Pa. The rotor RPM were sensed via inductive type sensor. All quantities were acquired via DAQ system based on NI CompactDAQ chassis, including relevant modules.

6.2. Measured data

The measurement was scheduled for 14 steady-state points. Each point was measured for the time of 180 s. This time is acceptable because its value fully corresponds with the assumption in Li et al. (2018). The revolution velocity step was 500 rpm (Table 2). Based on Hughes and Hase (2010), the Gaussian distributions of the measured variables were plotted, and the distribution confirmed the measurement and ruled out the errors (see Figure 11).

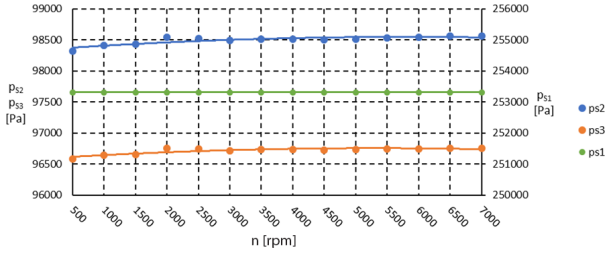

Figure 10. Static pressure data plot

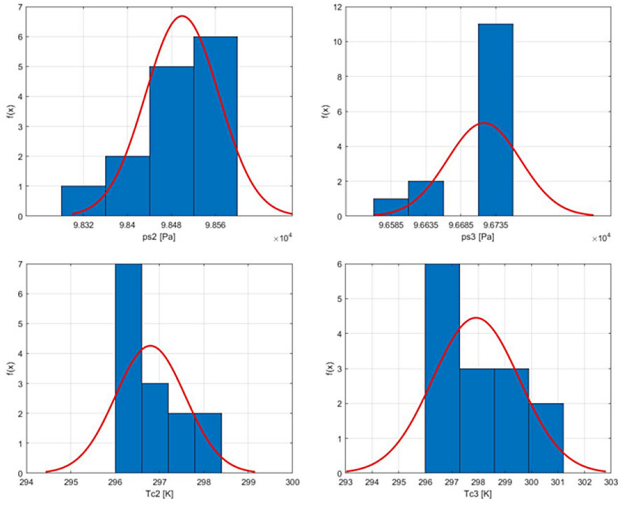

Figure 11. Measured data Gaussian distribution

Table 2. Steady state points

Steady state point	Rotating speed [rpm]
1	500
2	1000
3	1500
4	2000
5	2500
6	3000
7	3500
8	4000
9	4500
10	5000
11	5500
12	6000
13	6500
14	7000

At one steady-state point, the average value of all parameters from 180 s long data series was evaluated. The 2nd polynomial trendlines between the steady-state points were used. Figure 10 shows approximately constant values of static pressure. In the inlet is pressure of 253000 Pa, and on the left side (index 3) the pressure is 96718 Pa and on the right side (index 2) is 98500 Pa. Figure 12 shows the total temperature increasing through the rotating speed. In thermocouple 3 (T_{C3}), the temperature increased to 300.8 K, and in thermocouple 2 (T_{C2}) the total temperature increased to 298.2 K in maximal rotating speed of 7000 rpm.

$$\Delta p_S = p_{S2/3} - p_{S1}\,; \tag{4}$$

$$\Delta T_C = T_{C2/3} - T_{C1}\,. \tag{5}$$

The static pressure (Δp_S) and total temperature (ΔT_C) differences are calculated by Equation (4) and (5). The Figure 13 shows that the static pressure difference is ~–53 Pa

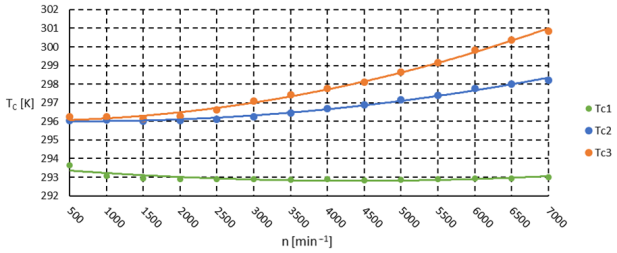

Figure 12. Total temperature data plot

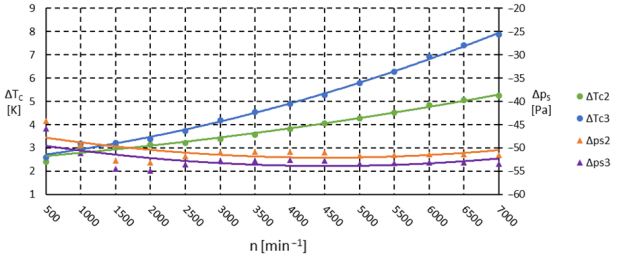

Figure 13. Static pressure and total temperature data differences

in both probes at all rotating speeds. The chart shows that the measured static pressures are in constant value at different speeds. This is an expected value because the flow expands to the ambient, and the static pressure probes are closed to the ambient. The total temperature difference in Figure 13 for the highest rotating speed is ~5 K in thermocouple 2 (ΔT_{C2}) and ~8 K in thermocouple 3 (ΔT_{C3}). The total temperature in thermocouple 2 increasing is higher than in thermocouple 3 by ~3 K. The difference between the thermocouples 2 and 3 is within sensor tolerance and acceptable. The measurement is thus correct because the error is negligible compared to standard practice. Figure 11 shows that the uncertainty is acceptable. Generally, the total temperature difference corresponds with the CFD calculation.

6.3. Results discussion

The shaft revolution speed range was considered according to the real aircraft turbine engine service conditions. The unexpected result from CFD is related to the total temperature behavior under different rotating speed regimes. The temperature difference between the first and last teeth is 37 K at a maximal rotating speed of 36000 rpm with small proportional radial clearance RCP. The static pressure difference meets expectations. The measurement was scheduled based on CFD simulations activities. The static pressure probes and the total temperature thermocouples in the inlet and the outlet of the measurement labyrinth seal were used. The CFD and measurement static pressure trendlines comparison are showed in Figure 12. The total temperature trendlines comparison are visible in Figure 13 for different values of rotating speed. The comparison between CFD simulation and experimental results for static pressure and total temperature absolute values is also introduced. It is given by the measurement boundary conditions, e.g., the pressure loss in inlet pressure air. However, from the qualitative point of view, the trend confirmed monitored quantities.

The CFD trendline with RCP = 0.15 (green line in CFD charts) is in all previous charts because the geometry fully corresponds with the measurement device.

The pressure loss in the inlet device is the reason there are differences between measurement and CFD. The total temperature differences between measurement and CFD are negligible. All differences are shown in Figure 16.

The 2nd-degree polynomial trendlines of all parameters were used. In the Table 3 there are shown the constants of the trendlines. The findings are as follows:

- The static pressure decreasing is evident from both CFD and the evaluation measurement. It is confirmation that the labyrinth seal works properly – like in CFD and measurement – exactly according to the theory in Sultanian (2018);
- The total temperature is increasing. This is mainly due to the relatively small proportional radial clearance in the aircraft turbine engine, high rotational speed (e.g., n = 36000 rpm) and fully developed rotating swirl between labyrinth teeth.

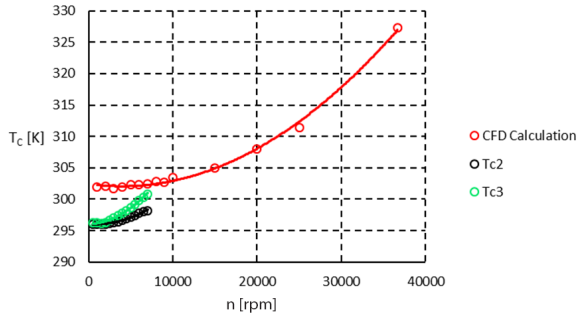

Figure 15. Total temperature comparison

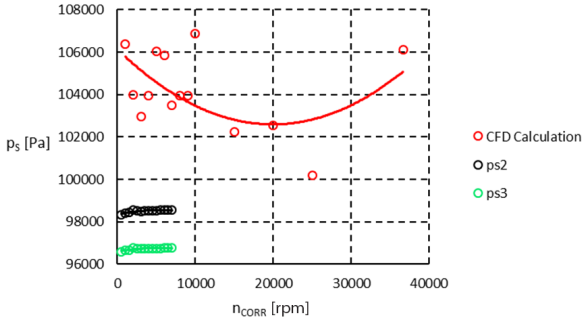

Figure 14. Static pressure comparison

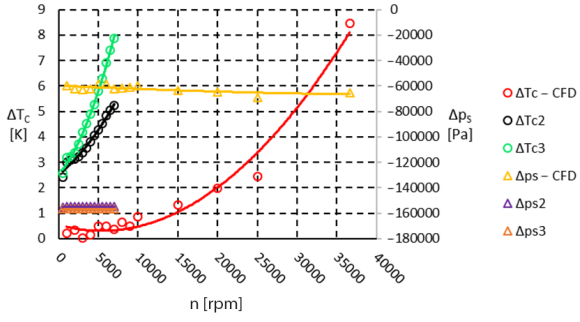

Figure 16. Static pressure and total temperature comparison

Table 3. 2nd degree polynomial trendlines constants

Trendlines comparison	A	B	C
Δp_S – CFD [Pa]	0.000003	–0.297887	–59643.107007
Δp_{S2} [Pa]	–0.000006	0.071534	–154969.751085
Δp_{S3} [Pa]	–0.000006	0.064439	–156725.597852
ΔT_C – CFD [K]	0.000001	–0.000086	0.539076
ΔT_{C2} [K]	0.000001	0.000241	2.526083
ΔT_{C3} [K]	0.000001	0.000359	2.521404

From Table 3 is possible to see that the constants are similar for both CFD and test results. Due to test hardware limits (i.e. maximal rotational speed), it was not possible to reach the maximal speed like in a real aircraft turbine engine in the service. This circumstance is a good task for future research.

Conclusions

New knowledge about labyrinth seal behavior was obtained and experimentally validated. The temperature in the seal is not constant as it was stated in previous studies, but the temperature increases with the radial clearance of the seal.

The results presented in the paper are thus of fundamental importance for turbomachinery design. Especially materials selection, dimensioning, stress and fatigue planning can be accomplished more accurately. This knowledge can have a direct effect on aircraft performance parameters.

Further experimental validation in broader operating conditions range will take place in new studies. Next research activities will lead up mainly to vortex structures description. The new methodology is being prepared for this purpose.

Acknowledgements

Authors acknowledge support from the ESIF, EU Operational Program Research, Development and Education, and the Center of Advanced Aerospace Technology (CZ.02.1.01/0.0/0.0/16_019/0000826), Faculty of Mechanical Engineering, Czech Technical University in Prague.

References

Ansys. (2016). *ANSYS Help Viewer 18.0*. https://ansyshelp.ansys.com/account/secured?returnurl=/Views/Secured/corp/v201/en/wb2_help/wb2_help.html%23wb2_help

Bloch, H. P., & Singh, M. P. (2009). *Steam turbines design, application and rerating*. McGraw-Hill.

Campagnoli, E., & Desando, A. (2019). Validation of a CFD Model of a labyrinth seal for low pressure turbines using a fluid-thermal tool tuned through experimental measurements. *Instrumentation Mesure Métrologie*, *18*(6), 509–516. https://doi.org/10.18280/i2m.180601

Childs, P. R. N. (2001). *Practical temperature measurement*. Butterworth-Heinemann. https://doi.org/10.1016/B978-075065080-9/50001-0

Chorin, A. J. (1968). Numerical solution of navier-stokes equations. *Mathematics of Computation*, *22*, 745–762. https://doi.org/10.1090/S0025-5718-1968-0242392-2

Čížek, M., & Pátek, Z. (2020). On CFD investigation of radial clearance of labyrinth seals of a turbine engine. *Acta Polytechnica, 60*(1). https://doi.org/10.14311/AP.2020.60.0038

Čížek, M., Vampola, T., & Popelka, L. (2020a). Comparison of labyrinth seal calculation and real aircraft turbine engine measurement. In *Proceedings of Topical Problem of Fluid Mechanics 2020* (pp. 19–26). Prague. https://doi.org/10.14311/TPFM.2020.003

Čížek, M., Pátek, Z., & Vampola, T. (2020b). Aircraft turbine engine labyrinth seal CFD sensitive analysis. *Aerospace Science and Engineering, 10*(19), 6830. https://doi.org/10.3390/app10196830

Čížek, M., & Vampola, T. (2020). Labyrinth seal of aircraft turbine engine air flow calculation at High Viskosity. *Acta Mechanica Slovaca, 23*(4), 6–12. https://doi.org/10.21496/ams.2020.011

Denecke, J., Schramm, V., Kim, S., & Wittig, S. (2002). Influence of rub-grooves on labyrinth seal leakage. In ASME *Turbo Expo 2002, Power for Land, Sea, and Air* (Vol. 3, pp. 771–779). ASME. https://doi.org/10.1115/GT2002-30244

European Aviation Safety Agency. (2014). *Type certificate data sheet*, *GE M601/H80 series turboprop engines*. https://www.easa.europa.eu/document-library/type-certificates/engine-cs-e/easae070-ge-m601h80-series-turboprop-engines

Fürst, J. (2016). Numerical simulation of flows through Labyrinth seals. *Applied Mechanics and Materials, 821,* 16–22. https://doi.org/10.4028/www.scientific.net/AMM.821.16

Hughes, I., & Hase, T. (2010). *Measurements and their uncertainties: A practical guide to modern error analysis*. Oxford University Press.

Ilieva, G. (2016). Labyrinth seals – a promising and effective design. *International Journal of Science and Research*, *5*(4). https://doi.org/10.21275/v5i4.NOV162352

Ilieva, G., & Pirovsky, C. (2019). Labyrinth seals with application to turbomachinery. *Materials Science & Engineering Technology, 50*(5), 479–491. https://doi.org/10.1002/mawe.201900004

Jia, X., Zhang, H., Zheng, Q., Fan, Sh., & Tian, Z. (2019). Investigation on rotor-labyrinth seal system with variable rotating speed. *International Journal of Turbo & Jet-Engine, 36*(1). https://doi.org/10.1515/tjj-2016-0066

Kerrebrock, J. L. (1992). *Aircraft engines and gas turbines*. Massachusetts Institute of Technology.

Kmoch, P. (2002). *Aircraft engines theory*. University of Defence in Brno.

Kurzke, J., & Halliwell, I. (2018). *Propulsion and power*. Springer. https://doi.org/10.1007/978-3-319-75979-1

Li, Y., Zhang, Z., Hao, X., & Yin, W. (2018). A measurement system for time constant of thermocouple sensor based on high temperature furnace. *Applied Sciences*, *8*(12), 2585. https://doi.org/10.3390/app8122585

Martin, H. M. (1908). Labyrinth packings. *Engineering, 85,* 35–38.

Romanik, G., Jaszak, P., & Rogula, J. (2019). Cooperation of the PTFE sealing ring with the steel ball of the valve subjected to durability test. *Open Engineering, 9*(1). https://doi.org/10.1515/eng-2019-0028

Selvaraji, M., Sam, P. J., & Nirmal, N. (2007). Optimization of labyrinth seal for screw compressor. In *ASME/JSME 2007 Thermal Engineering Summer Heat Transfer Conference* (Vol. 1, pp. 969–975). Vancouver, British Columbia, Canada. https://doi.org/10.1115/HT2007-32275

Stoff, H. (1980). Incompressible flow in a labyrinth seal. *Journal of Fluid Mechanics, 100*(4). https://doi.org/10.1017/S0022112080001437

Subramanian, S., Sekhar, A. S., & Prasad, B. V. S. S. S. (2015). Influence of combined radial location and growth on the leakage performance of a rotating labyrinth gas turbine seal. *Journal of Mechanical Science and Technology, 29*(6), 2535–2545. https://doi.org/10.1007/s12206-015-0545-8

Sultanian, B. K. (2018). *Gas turbine: Internal flow systems modeling*. Cambridge University Press. https://doi.org/10.1017/9781316755686

Ščeglajev, A. V. (1983). Steam turbines. *Státní nakladatelství technické literatury.* Czech Technical Books Publishing.

Tong, S. K., & Kyu, S. Ch. (2009). Comparative analysis of the influence of labyrinth seal configuration on leakage behavior. *Journal of Mechanical Science and Technology, 23*(10). https://doi.org/10.1007/s12206-009-0733-5

Wu, T., & Andrés, L. S. (2018). Leakage and dynamic force coefficients for two labyrinth gas seals: Teeth-on-Stator and interlocking teeth configurations. A computational fluid dynamics approach to their performance. *Engineering for Gas Turbines and Power, 141*(4). https://doi.org/10.1115/GT2018-75205